A Hybrid Magnetic Focusing System for Microwave Tubes

Elio A. Périgo, Joaquim J. Barroso, and Cláudio C. Motta, *Member, IEEE*

***Abstract*—By using a three-dimensional particle-in-cell code, this paper reports on the electron-beam propagation behavior in a drift tube under two situations. First, it investigated the influence of the acceleration potential on the beam trajectory when using a periodic permanent magnet (PPM) focusing structure upon keeping constant either the electric current or the beam perveance. Next, taking for granted the optimum focalization parameters found in the previous evaluation, it examined the feasibility of using a hybrid magnetic focusing system (HS)—a PPM array clamped at the ends by a pair of solenoids—so that the value of the magnetic flux density at the entrance to the PPM system satisfies the Brillouin field condition. An experimental setup of the HS using PPM NdFeB permanent magnets without pole pieces is also reported.**

***Index Terms*—Hybrid magnetic focusing system (HS), particle-in-cell (PIC) code, periodic magnetic focusing, traveling-wave tubes.**

I. Introduction

A KNOWLEDGE of the behavior of an electron beam propagating in a periodic permanent magnet (PPM) focusing structure is an inherent requirement in the design of microwave tubes such as klystrons amplifiers and traveling-wave tubes (TWTs). Differing from a uniform focusing structure, such as solenoids, PPM focusing structures can present stopbands and electron-beam propagation cutoff.

Several works using computational codes have been reported, which present the development of new models of klystrons and TWTs or even improvement of their performance [1]–[3]. However, one of the most important design parameters with a strong impact on the microwave tube operation is the electron-beam acceleration potential V_0. Examples of its influence are directly assessed upon an analysis of the beam dynamics in the focusing structure.

Considering the Brillouin system where the cathode is magnetically shielded, the required peak magnetic field to focus a given electron beam scales with $V_0^{-1/4}$.[1] Meanwhile, when using a PPM structure, it is known that α, which varies with V_0^{-1}, quantifies the degree of beam transmission along the drift tube. Therefore, the acceleration potential becomes an especially relevant parameter once the peak magnetic flux density B_0 has already been specified [3].

Furthermore, for saving weight and bulk, it is desirable to replace a focusing system based on a solenoid by a PPM structure. Yet, sometimes due to mechanical restrictions on microwave tubes, the magnetic flux density at the entrance of the PPM may present a different value from the Brillouin field. To our knowledge barely studied, a solution proposed here is a hybrid combination of a PPM array clamped between a pair of solenoids, each one located at the ends of the PPM stack, from now on referred to as hybrid magnetic focusing system (HS). As will be shown, this structure ensures that the magnetic-field pattern conforms with the Brillouin focusing theory so that the electron beam can be confined stably.

On the basis of code KARAT [4],[2] this paper examines the behavior of an electron beam propagating in a drift tube using a PPM focusing structure for two cases. First, with a constant electric current of $I_0 = 24$ A and, second, with a constant perveance of 0.77 μPerv. For both cases, the acceleration potentials range from 15 to 125 kV. Later, at $V_0 = 100$ kV and $I_0 = 24$ A, it investigated the feasibility of the proposed HS, which consists of two solenoids and a PPM array with 22 NdFeB magnets (the same of previous cases). Results of an experimental setup of an HS to be used on a power helix TWT are also reported.

This paper is organized as follows. Section II gives a brief description of the simulations carried out and analyzes the

Manuscript received September 30, 2005; revised December 28, 2005. This work was supported in part by the State of São Paulo Research Foundation (FAPESP) under Grant 03/03586-4.

E. A. Périgo is with the Nuclear and Energetic Research Institute, São Paulo 05522-970 SP, Brazil (e-mail: eaperigo@yahoo.com).

J. J. Barroso is with the Associated Plasma Laboratory, National Institute for Space Research, São José dos Campos 12245-970 SP, Brazil (e-mail: barroso@plasma.inpe.br).

C. C. Motta is with the Brazilian Navy Technology Center at São Paulo, São Paulo 05508-900 SP, Brazil (e-mail: ccmotta@usp.br).

Digital Object Identifier 10.1109/TPS.2006.881888

[1]For Brillouin flow to occur, the beam must enter the magnetic field on axis with no radial electron motion and with a radius equal to the equilibrium radius, i.e., the radius at which space-charge forces are balanced by magnetic forces. The equilibrium condition in the radial direction is a balance of outward forces $-eE_r = r\rho_0/2\varepsilon_0$ due to space charge and $m\omega_L^2 r$ due to centrifugal acceleration against the inward magnetic radial force $e\omega_L r B_z$, where $\omega_L = (eB_z/2m)$ is the Larmor frequency. Then, by equating the oppositely directed radial forces and expressing the charge density by means of $\rho_0 = (I_0/(\pi a^2 v_z))$, where v_z is the axial beam velocity and I_0 is the total current enclosed within the equilibrium radius a, it is obtained $B_z = (2I_0/(\pi\eta\varepsilon_0 v_z))^{1/2}/a$. Since in the weakly relativistic limit $mv_z^2/2 = eV_0$, it can be seen that the confining magnetic field scales with the accelerating potential as $V_0^{-1/4}$.

[2]A fully electromagnetic code based on the particle-in-cell (PIC) method, the code KARAT has been under continuous development for over twenty years, and applied successfully to many physical problems (e.g., the magnetically insulated diode, the limiting current problem, the reditron, transient wave processes inside inhomogeneous waveguide, microwave generation, and chaotic processes). Also, comparison with analytical solutions has been found in excellent agreement.

TABLE I
PARAMETERS FOR SIMULATIONS USING THE CODE KARAT

Parameter	Value	Unit
B_0	173	mT
Drift tube – length	8.5	cm
Drift tube – radius	1.0	cm
Beam radius	0.18	cm

effect of the acceleration potential V_0 on the magnetic-field parameter α. Section III discusses the simulation results for the beam propagation and compares theoretical and experimental data of the PPM and HS built. Section IV summarizes this paper.

II. SIMULATIONS

The system is axially symmetric in which a solid electron beam is generated from a completely magnetic shielded cathode, with all electron trajectories being parallel to each other at the entrance of the drift tube, with a 1.0-cm radius and 31.0-cm long. In analyzing the influence of both the initial dispersions of the thermal energy (ranged between 0–10 eV) and the polar angle (ranged between 0°–15°) of the electrons leaving the cathode surface, it was verified that about 93% of the beam would reach the collector in all situations analyzed. Without including initial dispersion on the beam formation, therefore, the PPM results that follow refer to the first quarter of the tube, whereas full-length simulations are performed for the HS. The physical system is run on a spatial grid of square cells 0.05-cm size with over 20 000 macroparticles representing the beam electrons.

The effect of self-space charge on the beam equilibrium is calculated self-consistently by the code. As the beam propagates, a potential difference between the beam and the drift tube (at a zero potential) gradually develops due to the space charge in the beam. In addition, the self-space-charge depression produces a potential drop across the beam which results in a finite energy spread, and all these effects are properly taken into account throughout the simulations.

Referring to a nonthermal beam with parameters given in Table I, the simulation results will be discussed based on the magnetic-field parameter α and the space-charge parameter β, which are defined in [5], where η is the electron charge-mass ratio, K is the beam perveance, ε_0 is the free-space electrical permitivitty, a is the beam radius, L is the PPM period, and V_0 is the beam accelerating potential.

$$\alpha = \frac{\eta B_0^2 L^2}{64\pi^2 V_0} \tag{1}$$

$$\beta = \frac{\eta K L^2}{8\pi^3 \varepsilon_0 a^2 (2\eta)^{3/2}}. \tag{2}$$

The magnetic density flux on-axis, used during the KARAT simulations, was obtained by means of a computational code developed by the group. This code utilizes analytical expressions to determine the field profile of permanent magnets (from volumetric and superficial magnetic charge densities) [6] and solenoid sections (from direct integration of Biot-Savart law). In both cases, the condition $\nabla \cdot \vec{B} = 0$ holds within an absolute error tolerance of 10^{-6}. Besides, the PIC code also tests the condition $\nabla \cdot \vec{B} = 0$ and, if it is not satisfied, a routine outputs an error message and the simulation halts. The theoretical contribution of both PPM and solenoid fields was carried out using the superposition principle.

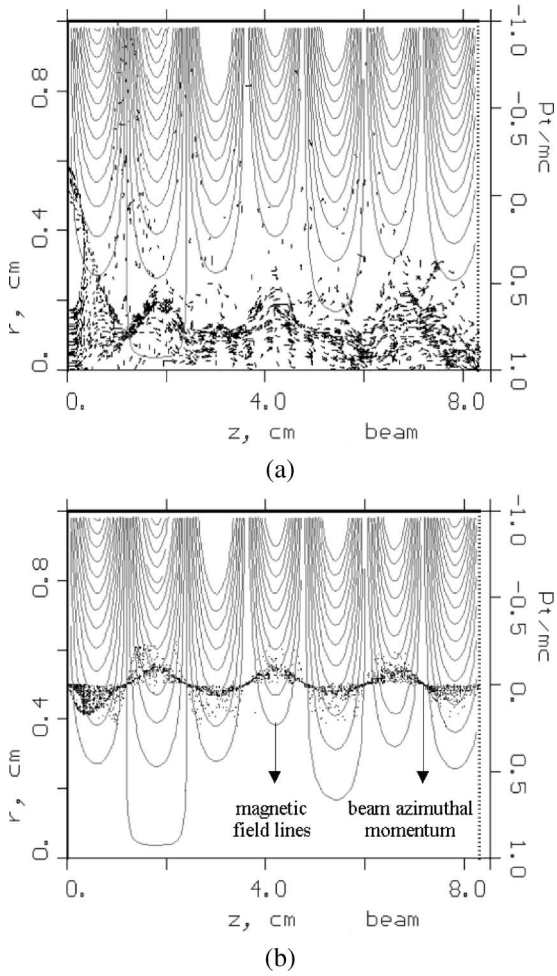

Fig. 1. Electron-beam propagation profile with $V_0 = 15$ kV and $B_0 = 173$ mT in (a) and azimuthal momentum plot in (b). The magnetic-field lines of the PPM structure are also shown ($\alpha = 0.320$ and $\beta = 0.893$).

Upon examining the effect of the magnetic-field parameter α on the beam dynamics, the acceleration potential is varied in the 15–100-kV range, with axial magnetic density flux peak $B_0 = 173$ mT and magnetic period $L = 2.4$ cm kept constant in (1). For small values of V_0, α is much larger than the value reported in literature that allows perfect focusing of an electron beam [7]. Thus, for low V_0 values, one expects no transmission along the drift tube. In fact, $V_0 \cong 7$ kV gives a too large α value of 0.66, which rapidly decreases with increasing acceleration potential. From $V_0 = 20$ kV ($\alpha = 0.24$), the change in α is small compared with the previous situation, while for V_0 up to 100 kV, the magnetic-field parameter α becomes essentially constant.

III. RESULTS AND DISCUSSION

A. Current Constant

The behavior of electron beams with the same electric current of $I_0 = 24$ A, but subject to different acceleration potentials, is

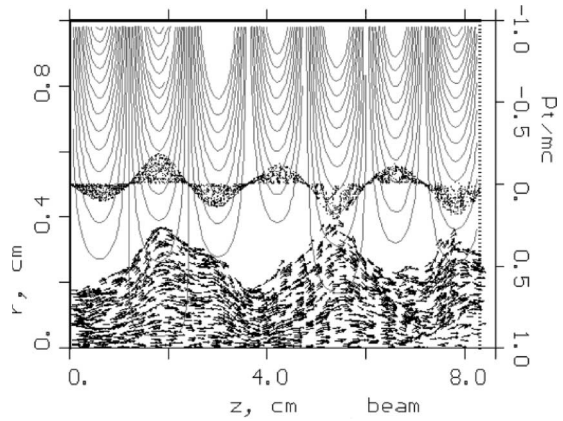

Fig. 2. Electron-beam path for $V_0 = 30$ kV and $B_0 = 173$ mT. The magnetic-field lines of the PPM structure and the azimuthal momentum plot are also shown ($\alpha = 0.160$ and $\beta = 0.316$).

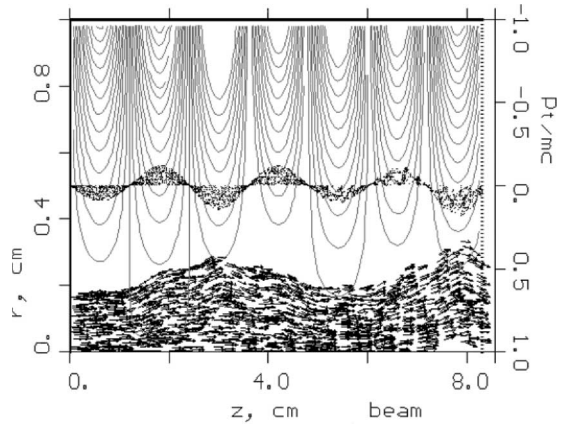

Fig. 3. Electron-beam path for $V_0 = 50$ kV and $B_0 = 173$ mT. The magnetic-field lines of the PPM structure and the azimuthal momentum plot are also shown ($\alpha = 0.096$ and $\beta = 0.147$).

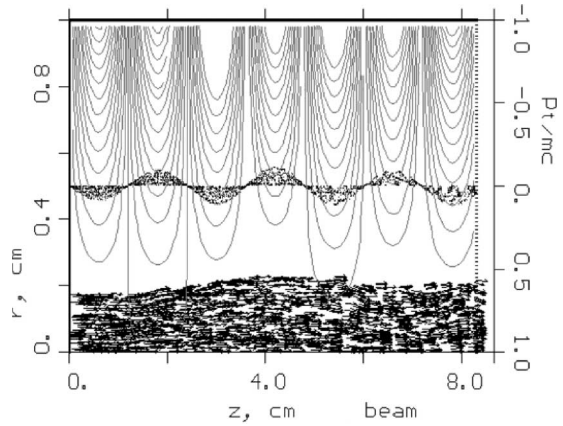

Fig. 4. Electron-beam path for $V_0 = 75$ kV and $B_0 = 173$ mT. The magnetic-field lines of the PPM structure and the azimuthal momentum plot are also shown ($\alpha = 0.064$ and $\beta = 0.080$).

presented in Figs. 1–6. When $V_0 = 15$ kV (see Fig. 1), it can be noticed that there is no satisfactory transmission of the electron beam along the drift tube. This can be explained by considering the reduced velocity imparted to the beam by the acceleration potential. Analyzing the electron-beam propagation when $V_0 = 30$ kV as shown in Fig. 2, one can notice that the confinement

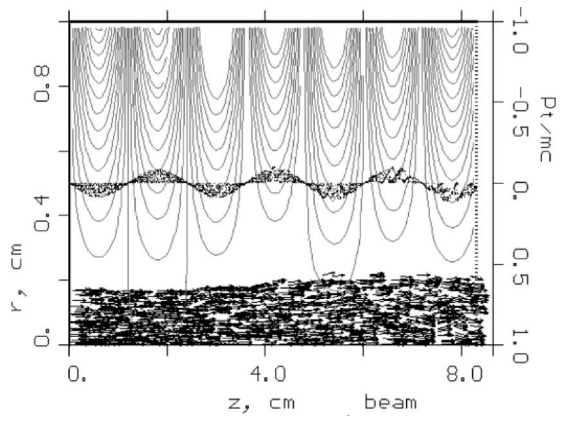

Fig. 5. Electron-beam path for $V_0 = 100$ kV and $B_0 = 173$ mT. The magnetic-field lines of the PPM structure and the azimuthal momentum plot are also shown ($\alpha = 0.048$ and $\beta = 0.052$).

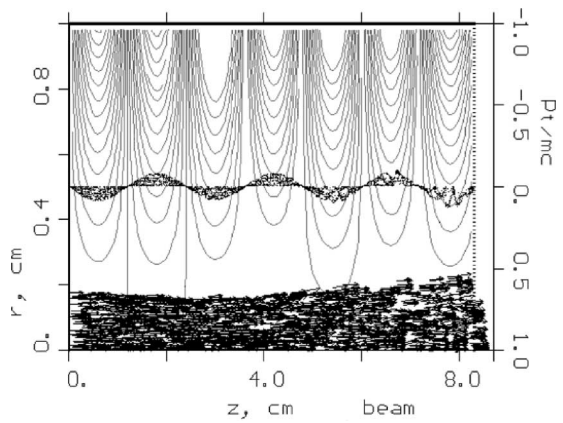

Fig. 6. Electron-beam path for $V_0 = 125$ kV and $B_0 = 173$ mT. The magnetic-field lines of the PPM structure and the azimuthal momentum plot are also shown ($\alpha = 0.038$ and $\beta = 0.037$).

is unsatisfactory because $\beta > \alpha$ and also due to an initial beam spreading.

When $V_0 = 50$ kV, as shown in Fig. 3, one can verify that beam transmission through the drift tube takes place. However, the beam radius reaches unacceptable values (about 0.3 cm when $z = 3.0$ cm) compared with its design dimension because of edge electron ripple (RF signal amplification will depend on the radial dimension of the electron beam). When $V_0 = 75$ kV, shown in Fig. 4, it is apparent that the beam ripple gets smaller and the electric space charge flux is more homogeneous. This situation is closer to the ideal one, in which the beam radius becomes nearly constant along the axial distance. In this case, the magnetic density flux counterbalances the space charge force almost totally. The parameter α is about 0.064, and this value must be as small as possible because RF field defocusing forces are not yet being considered.

Analyzing Fig. 5, for which $V_0 = 100$ kV, the beam profile resembles that shown in Fig. 4. Although the variation of the acceleration potential is about 33% higher, the electron-beam profile is almost unchanged. On the other hand, for $V_0 = 125$ kV (see Fig. 6), one can note that although a ripple still persists, the beam-radius variation is acceptable experimentally, and this situation turns out attractive to be implemented.

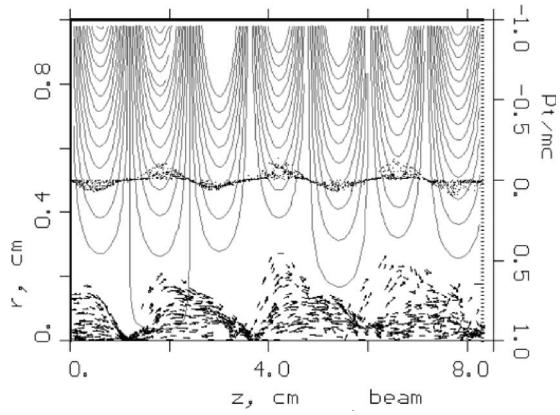

Fig. 7. Electron-beam path for $V_0 = 15$ kV and $B_0 = 173$ mT. The magnetic-field lines of the PPM structure and the azimuthal momentum plot are also shown ($\alpha = 0.320$ and $\beta = 0.053$).

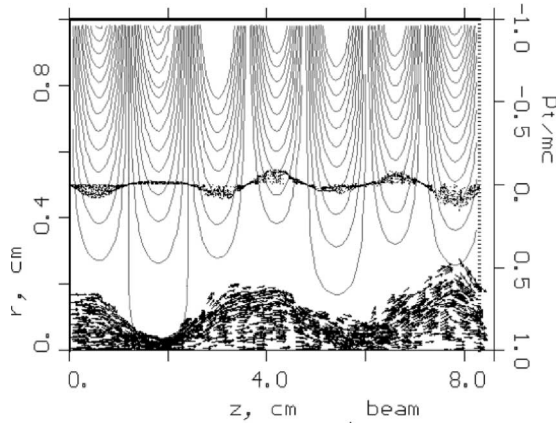

Fig. 8. Electron-beam path for $V_0 = 30$ kV and $B_0 = 173$ mT. The magnetic-field lines of the PPM structure and the azimuthal momentum plot are also shown ($\alpha = 0.160$ and $\beta = 0.053$).

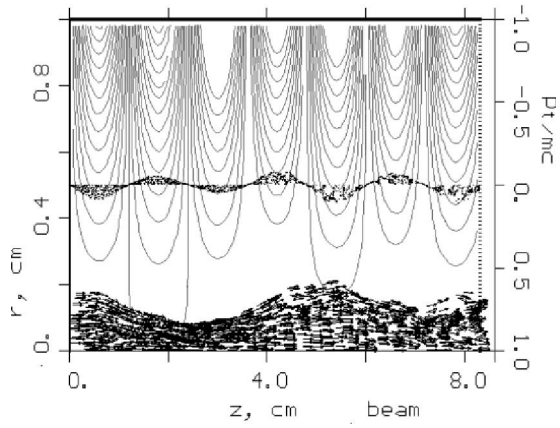

Fig. 9. Electron-beam path for $V_0 = 50$ kV and $B_0 = 173$ mT. The magnetic-field lines of the PPM structure and the azimuthal momentum plot are also shown ($\alpha = 0.096$ and $\beta = 0.053$).

B. Perveance Constant

It is presented, in Figs. 7–11, the electron-beam propagation profile together with the azimuthal momentum plot and PPM magnetic-field lines, when V_0 is increased from 15 to 125 kV, keeping constant the perveance $K = 0.77$ μPerv ($K = I_0/V_0^{3/2}$ ratio).

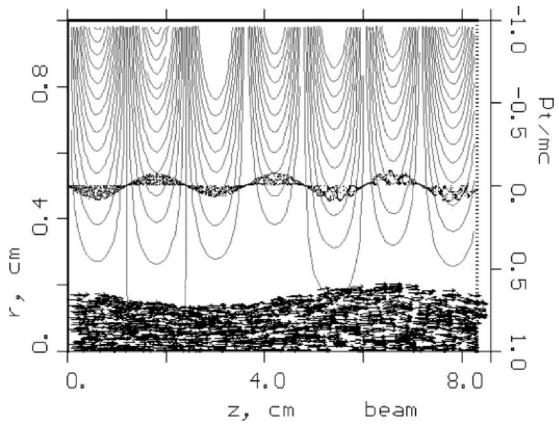

Fig. 10. Electron-beam path for $V_0 = 75$ kV and $B_0 = 173$ mT. The magnetic-field lines of the PPM structure and the azimuthal momentum plot are also shown ($\alpha = 0.064$ and $\beta = 0.053$).

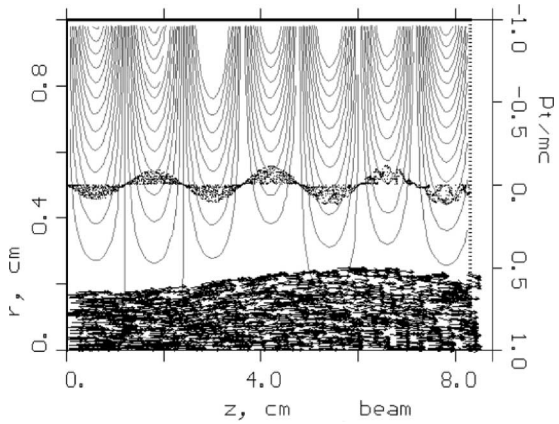

Fig. 11. Electron-beam path for $V_0 = 125$ kV and $B_0 = 173$ mT. The magnetic-field lines of the PPM structure and the azimuthal momentum plot are also shown ($\alpha = 0.038$ and $\beta = 0.053$).

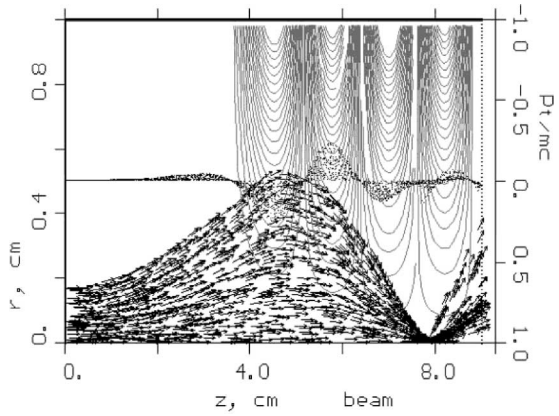

Fig. 12. Electron-beam paths for $V_0 = 100$ kV, $I_0 = 24$ A, and $B_0 = 173$ mT when only the PPM structure is operating. The magnetic-field lines of the PPM structure and the azimuthal momentum plot are also shown.

It can be seen that V_0 values in the 15–50-kV range lead to an initial beam convergence, with the undulating electron beam propagating downstream the drift tube, as shown in Figs. 7–9. But increasing the acceleration potential (and also the electric current to maintain the perveance unchanged), the beam flux

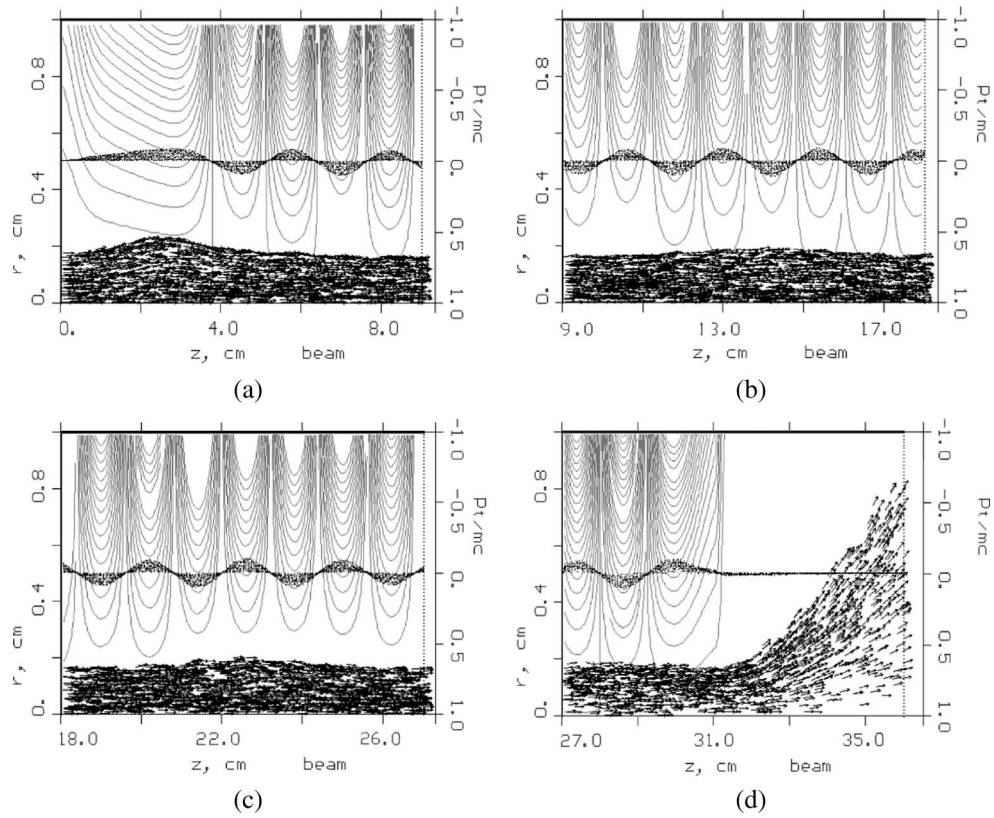

Fig. 13. Electron-beam paths for $V_0 = 100$ kV, $I_0 = 24$ A, and $B_0 = 173$ mT along 31.0 cm. The magnetic-field lines of the PPM structure and the azimuthal momentum plot are also shown.

gets more laminar, and a suitable configuration is obtained at $V_0 = 75$ kV, as shown in Fig. 10.

Above this acceleration potential, the space-charge parameter β becomes larger than the magnetic-field parameter α, because α goes as the inverse of V_0. For an acceleration potential of 125 kV, corresponding to Fig. 11, there is an initial beam spread resulting from a further increase of the space-charge parameter.

C. HS

Overlaid with the phase-space plot of the azimuthal momentum, Fig. 12 presents the electron beam propagating under the action of the PPM just developed, and Fig. 13(a)–(d) shows the beam trajectory when the designed HS is operating. This system includes two sections of a multisection solenoid reported elsewhere [8], [9].

When only the PPM structure is acting on the electron beam, as shown in Fig. 12, the beam electrons diverge due to space-charge forces, which are stronger than the magnetic forces developing along $0 \leq z \leq 4.0$ cm (there exists a B_z in this region, but with magnitude much lower than the peak value generated by the permanent magnet stack, and for this reason, the corresponding B_z lines are not shown in Fig. 12). The beam reaches a maximum radius of about 0.5 cm and, certainly, the charges would hit the TWT slow-wave structure. Following the spreading, the beam is strongly focused because of the PPM action, with a lack of synchronism between the electron axial momentum and the periodic magnetic field.

On the other hand, when the HS is operating on the electron beam, as shown in Fig. 13(a), the beam starts flowing with a radius of 0.18 cm, with the radial spread noticed in the $2.0 \leq z \leq 4.0$-cm interval being attributed to the low magnetic density flux. These B_z values arise from the superposition of the fields produced by the solenoids and the PPM stack, specially the magnets positioned at the entrance of the drift tube. An interesting fact that must be discussed refers to the electron-beam azimuthal momentum. On the left, in the region where the magnetic field is predominantly due to the solenoid (see the magnetic-field lines), it can be noticed that the azimuthal momentum continually increases because there are no changes in the direction of B_z, as shown in Fig. 12. For $z \cong 4.0$ cm, the axial component of the magnetic density flux becomes null, indicating the beginning of the periodic profile of B_z, and the azimuthal momentum, in this point, is zero. From this point on, the beam starts spinning with alternate clockwise and counterclockwise circular motions, a feature of PPM systems.

Analyzing in Fig. 13(b), the second segment of the 31.0-cm long drift tube, it is verified that the electron-beam propagation reaches a steady profile, as well as the distribution of the azimuthal momentum. In the third region simulated, as shown in Fig. 13(c), it can be noticed the beginning of a spreading with the beam reaching a radius of about 2.0 cm at $z \cong 22.5$ cm. This spreading does not hinder the TWT operation, because no beam interception occurs on the slow-wave structure.

Fig. 13(d) shows the last simulation region during the investigation of the HS. Some difference exists on the magnetic-field lines. The first two magnetic-field patterns refer to the

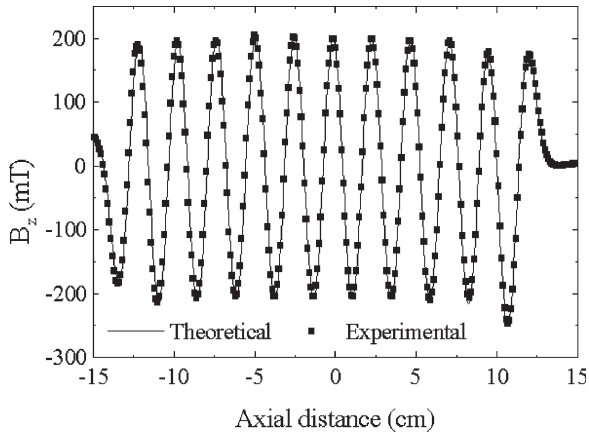

Fig. 14. Comparison between theoretical and experimental axial field B_z of the designed PPM system.

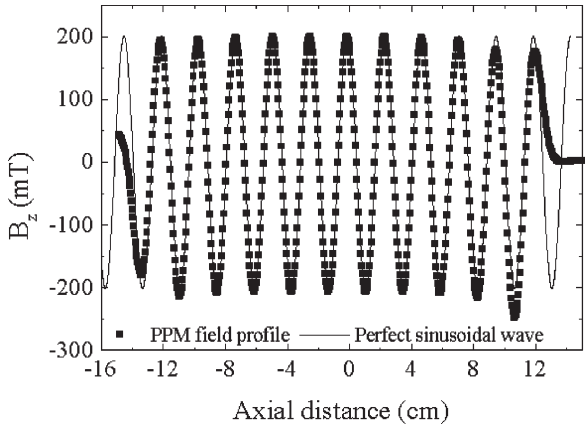

Fig. 15. Comparison between a perfect sinusoidal wave and the experimental axial field B_z of the designed PPM system.

magnets, while the rightmost one originates from the second HS solenoid placed on the right of the stack. At exit, the electron beam converges and, after that, spreads out over the collector region because there is no applied magnetic field there, and the azimuthal momentum vanishes as expected. The region where the spreading occurs ($z \cong 5.0$ cm) corresponds to the position of the TWT collector, although it is not illustrated.

Finally, in dealing with the HS, we remark that the requirements to determine the peak axial magnetic flux density must be the same as in the Brillouin system, since in PPM designs, the HS is an additional setup that ensures beam propagation along the distance where the permanent magnets are located, upon satisfying the Brillouin focusing conditions.

D. HS—An Experimental Setup

This section describes the experimental HS that has been designed and built for application on a helix TWT of perveance $K = 0.77$ μPerv.

Fig. 14 compares theoretical and experimental profiles of the axial magnetic flux density component of the PPM array, without considering the solenoids placed at the ends of the stack. It can be seen that the agreement is excellent along the axis of symmetry ($\rho = 0$), with a discrepancy of about 2%. The end effect can also be noticed, where B_z overshoots at around $z = 11.0$ cm, as theoretically expected. Periodicity of B_z is kept constant over ten periods of length 2.4 cm as designed, along about 22.0 cm. Experimental data of the axial magnetic flux density has been obtained from a Hall probe GLOBALMAG TMAG-01T assembled on a two-dimensional precision table. The B_z profile was measured at steps of 0.1 cm.

Next, the PPM experimental B_z profile is compared with a sinusoidal waveform (with the same period of the periodic magnetic field) in Fig. 15. Except at the ends, as expected, excellent agreement is clearly apparent, showing that a PPM field might be described by a sinusoidal or cosinusoidal function.

Fig. 16 compares the calculated B_z profile with that measured on the experimental HS. Once again, it can be noticed that the agreement is very satisfactory, with a discrepancy of nearly 2% over an extension of 28.0 cm. Before the PPM field and with a peak of 83 mT, it can be seen the profile due to the

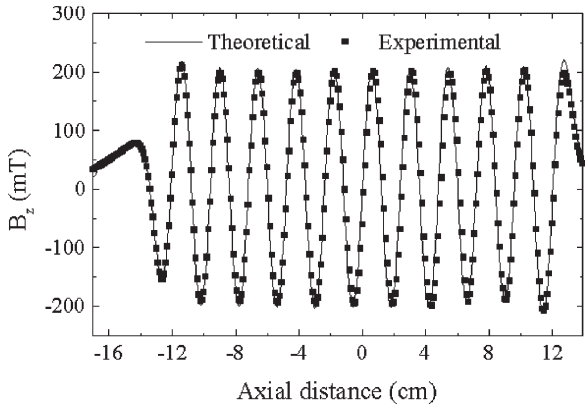

Fig. 16. Comparison between theoretical and experimental axial field B_z of the HS designed.

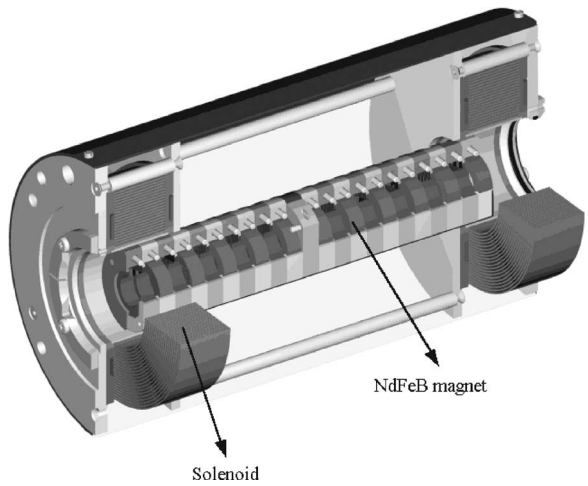

Fig. 17. Schematic drawing of the HS focusing system.

first solenoid, close to the TWT electron gun. At $z \cong 31.4$ cm where the axial magnetic flux density becomes null, the periodic profile unfolds and extends toward the collector.

Displayed in Fig. 17, this PPM is constituted of 22 NdFeB ring-shaped permanent magnets (number of peaks of the plot), with no ferromagnetic pole pieces being included, because the magnets themselves were powerful enough to produce the required axial magnetic flux density. Furthermore, one can

remark that there is no demagnetization of the permanent magnets as the compound intrinsic coercivity is higher than remanence ($B_r \cong 1.3$ T for all magnets).

IV. Conclusion

The effect of the acceleration potential on electron-beam propagation in a drift tube keeping the parameters of the magnetic focusing structure constant under two cases was discussed. It was verified that for small values of V_0, it is not possible to obtain a satisfactory focusing due to high values of the magnetic-field parameter. One could also infer that the magnetic density was not high enough to keep the beam radius constant, because this parameter depends on V_0. For acceleration potentials between 75 and 125 kV, it was possible not only to obtain a good transmission along the drift tube but also to notice a full correlation between the azimuthal momentum and the PPM field pattern.

When the perveance remained unchanged, it was verified that for low acceleration potentials (< 50 kV), no confined flow was possible, and between 75 and 125 kV, the beam propagation is acceptable for experimental evaluations.

The feasibility of the proposed HS was demonstrated upon examining the electron-beam propagation through a 31.0-cm long drift tube, although with occurrence of electric charge spread at the transition region between the first solenoid and the PPM. This spreading, however, does not affect the system efficacy, because the electrons kept their trajectory toward the collector with no beam interception. In addition, by employing only the PPM array as the focusing structure, it was impossible to keep the beam with a constant radius, even along the first quarter of the tube.

The theoretical and experimental profiles of the axial component of magnetic flux density of a PPM so far designed without pole pieces were compared and agreed to within 2%. The end effect was verified, for which B_z is sinusoidal or cosinusoidal (depending on the starting point analysis), with a period of 2.4-cm along a length of 22.0 cm.

References

[1] C. L. Kory, "Investigation of fully three-dimensional helical RF field effects on TWT beam/circuit interaction," *IEEE Trans. Electron Devices*, vol. 48, no. 8, pp. 1718–1726, Aug. 2001.

[2] ——, "Effect of geometric azimuthal asymmetries of PPM stack on electron beam characteristics," *IEEE Trans. Electron Devices*, vol. 48, no. 1, pp. 1718–1726, Aug. 2001.

[3] E. A. Périgo, J. J. Barroso, and C. C. Motta, "A power TWT PPM design using a 3-D PIC code," in *Proc. IVEC*, Apr. 2005, pp. 181–184.

[4] V. P. Tarakanov, *User's Manual for Code KARAT*. Springfield, VA: Berkeley Research Associates, 1994.

[5] B. N. Basu, *Electromagnetic Theory and Applications in Beam-Wave Electronics*. Singapore: World Scientific, 1996.

[6] E. A. Périgo, R. N. Faria, and C. C. Motta, "A fast approach to PPM design," in *Proc. IVEC*, Apr. 2005, pp. 361–364.

[7] A. M. Clogston and H. Heffner, "Focusing of an electron by periodic fields," *J. Appl. Phys.*, vol. 25, no. 4, pp. 436–447, Apr. 1954.

[8] E. A. Périgo, R. N. Faria, J. J. Barroso, and C. C. Motta, "Design of a multi-sections solenoid for power microwave tubes," in *Proc. IMOC*, Jul. 2005, pp. 233–236.

[9] E. A. Périgo, R. N. Faria, and C. C. Motta, "Construction and characterization of a multi-sections solenoid for power microwave tubes," in *Proc. IMOC*, Jul. 2005, pp. 226–228.

Elio A. Périgo was born in Santo André, Brazil, in 1981. He received the M.S. degree in nuclear technology from the Nuclear and Energetic Research Institute (IPEN), São Paulo, Brazil, in 2005. He is currently working toward the Ph.D. degree in materials engineering, specifically in hard magnetic materials.

His research interests include the development of permanent magnets, based on PrFeB and NdFeB compounds, and focusing systems for microwave tubes.

Joaquim J. Barroso received the B.Sc. degree in electrical engineering and the M.Sc. degree in plasma physics from the Technological Institute of Aeronautics, São José dos Campos, SP, Brazil, in 1976 and 1980, respectively, and the Ph.D. degree in plasma physics from the National Institute for Space Research (INPE), São José dos Campos, in 1988.

He has been with INPE since 1982 and has been involved in the design and construction of a high-power 32-GHz gyrotron. During 1989–1990, he was a Visiting Scientist with the Plasma Fusion Center, Massachusetts Institute of Technology, Cambridge. His current interests include high-power microwave generators and plasma technology.

Cláudio C. Motta (M'87) received the B.S. degree in electrical engineering from the College of Engineering of S. José dos Campos, SP, Brazil, the M.S. degree in plasma physics from the Technology Institute of Aeronautics (ITA), S. José dos Campos, and the Ph.D. degree in laser-plasma physics from the University of São Paulo (USP), in 1982, 1986, and 1996, respectively.

With the Brazilian Navy Technology Center (CTMSP) since 1987, he has been involved in the design and construction of power microwave tubes, and since 2002, he has been an Associate Professor with USP. His research interests include microwave electronics and laser-plasma technology.

Dr. Motta is a member of the Microwave and Optoelectronics Brazilian Society.